Structural studies of SO_2 adsorption on metal surfaces

1997 J. Phys.: Condens. Matter 9 3647

(http://iopscience.iop.org/0953-8984/9/18/006)

J. Phys.: Condens. Matter **9** (1997) 3647–3670. Printed in the UK PII: S0953-8984(97)68795-0

REVIEW ARTICLE

Structural studies of SO_2 adsorption on metal surfaces

Jochen Haase

Fritz-Haber-Institut der Max-Planck-Gesellschaft, Faradayweg 4–6, D-14195 Berlin, Germany

Received 19 November 1996, in final form 20 February 1997

Abstract. The adsorption and condensation of sulphur dioxide on a number of metal surfaces is examined with emphasis on the observed surface structures. First some properties of gas-phase SO_2 and the characteristic bonding modes of SO_2 in transition-metal complexes are summarized. The role of fast and high-resolution core-level spectroscopy in the study of the kinetics of surface processes and in the identification of surface species is demonstrated for SO_2 adsorption and temperature-dependent decomposition on Cu(100). Structural studies of SO_2 adsorption on Ag(110), Pd(100) and Pt(111) using qualitative techniques are reviewed as well as quantitative structure determinations of condensed SO_2 and of SO_2 adsorption on Ni(110), Ni(100), Ni(111) and Cu(100) using x-ray absorption fine structure. The different adsorption and desorption behaviour is discussed in the light of the electronic structure of both the adsorbate and the substrate.

1. Introduction

There are a number of stories to tell when dealing with sulphur dioxide. Among the many uses of minor importance, its disinfecting and fumigating efficacy, which has been known for a long time, may be mentioned. So Odysseus, after the slaughter of the suitors, calls the nurse [1]: 'Bring me sulphur, which cleanses all pollution, and fetch fire also that I may burn it, and purify the cloisters'.

Nowadays, huge quantities of poisonous SO_2 are formed by the combustion of fuels such as coal, oil and natural gas in power plants, factories and homes. As a consequence, SO_2 is a major air pollutant and its removal from combustion gases is of great importance. In industry, SO_2 is usually formed by burning naturally occurring sulphur or by roasting metal sulphides in air. SO_2 is mainly employed in the manufacture of sulphuric acid with the oxidation to SO_3, either photochemically or in the presence of catalysts (platinum), as the most important intermediate process. Similar reactions proceed in the atmosphere where H_2SO_4 is formed by oxidation of predominantly man-made SO_2 with the well known phenomenon of 'acid rain' in the northern hemisphere as a result. The oxidation of SO_2 to H_2SO_4 is also responsible for the corrosion of many metals by SO_2. The catalytic activity of most transition metals is drastically reduced by the presence of SO_2 or other sulphur-containing compounds at extremely low concentration in the reagents [2]. SO_2 adsorption on these metals, in particular on platinum, is thus important in key areas of catalysis, because platinum catalysts are used not only for catalytic combustion, but also for motor car emission control.

Physically, SO_2 is interesting mainly for three reasons. It has frequently been used as a model compound for studying vibration and rotation. Surface physicists, on the other hand, are attracted by its comparatively high electron affinity, which should result in a

0953-8984/97/183647+24$19.50

more pronounced π-acceptor behaviour in bonding to substrates than known from CO. Finally, SO_2 exhibits interesting properties as a ligand in transition metal complexes with an unequalled diversity of bonding modes [3], which could help to understand the bonding of SO_2 to metal surfaces.

Looking at this widespread importance of SO_2 it is surprising that until recently only little interest has been shown in the adsorption and reaction behaviour of SO_2 on single-crystal metal surfaces. Most of the comparatively few studies concentrated on the question of molecular versus dissociative adsorption and condensation and on the identification of adsorbed SO_x ($x \neq 2$) species as a result of SO_2 decomposition using temperature-programmed desorption (TPD), high-resolution electron energy loss spectroscopy (HREELS), work function measurements, UV photoelectron spectroscopy (UPS) and x-ray photoelectron spectroscopy (XPS). A crude general picture of SO_2 adsorption on metal surfaces derived from these studies shows spontaneous or thermally activated decomposition on all of them (Fe, Rh, W, Ni, Pd, Pt, Cu and Zn) except on Ag where SO_2 adsorbs and desorbs molecularly.

Until recently, however, no quantitative structure determination has been reported. This might be due to a number of different factors. First, the 'classic' experimental techniques for surface structure determinations—low-energy electron diffraction (LEED), surface-extended x-ray absorption fine structure (SEXAFS) with the related technique of near-edge x-ray absorption fine structure (NEXAFS) and photoelectron diffraction (PED)—have just started to collect data on molecular adsorption. Second, adsorbed SO_2 monolayers usually do not seem to exhibit long-range order and, if they do, the latter is rapidly destroyed by an electron beam [4]. LEED investigations are, therefore, either impossible or at least rather demanding. Finally, structural analyses turn out to be complex due to the three-atom adsorbate SO_2 and are often complicated by co-adsorbed decomposition products.

Some structural information has emerged from the application of qualitative experimental techniques such as HREELS, angle-resolved UPS (ARUPS) and NEXAFS and by making use of the surface-cluster analogy [5] and of molecular orbital analyses. Quite generally it is assumed that SO_2 bonds to the substrate through its S atom. On Pd(100) [6], Ag(110) [7, 8], Ni(110) [4] and Pt(111) [9] SO_2 has been suggested to adsorb with its molecular plane perpendicular to the surface and aligned along the $\langle 100 \rangle$ azimuth (perpendicular to the close-packed rows) in case of the (110) substrates (at low coverages). But whereas on Ag(110) SO_2 adsorbs with its C_2 axis perpendicular to the surface, this axis is tilted within the molecular plane for SO_2 on Pd(100), Ni(110) and Pt(111) with the tilt being attributed to an additional O–substrate bonding interaction. For all these systems the adsorption site could only be guessed. S locations in hollow sites on Pd(100) and Ni(110) were assumed, while on-top sites on Ag(110) and sites between on-top and bridge positions on Pt(111) were favoured.

Quite recently quantitative structure determinations of SO_2 adsorbed on Ni(111) [10], Ni(100) [10] and Ni(110) [11] and of the decomposition product SO adsorbed on Cu(100) [12], which revealed hitherto unobserved parallel orientations of the adsorbed SO_2 and SO species and unexpected adsorption sites, have been performed. All these structural studies used the x-ray absorption fine structure (XAFS) technique, which by combining the NEXAFS and SEXAFS results turns out to be especially powerful for complex molecular systems with no structural information beforehand. While NEXAFS yields the orientation of the molecular plane, SEXAFS measurements above the S and O K edge determine independently the locations of the S and O atoms, respectively.

The organization of the remainder of this article is as follows. In section 2 some structural and electronic parameters of gas-phase SO_2, which are relevant for the following

sections, are listed. Section 3 contains a brief review of SO_2 coordination chemistry. The decomposition of SO_2 on various metal surfaces and the identification of the decomposition products are discussed in section 4. In particular, fast and high-resolution core-level photoemission (XPS) data are reported. Structural results for SO_2 adsorption on Ag(110), Pd(100) and Pt(111) taken from studies using qualitative techniques are summarized in section 5. Section 6 described briefly the SEXAFS and NEXAFS formalism which will be applied in sections 7–9. The main body of results is presented in these sections. Multilayer (condensed SO_2) data are discussed in section 7. The structures of monolayers adsorbed on Ni(111), Ni(100) and Ni(110) are described in section 8. Section 9 contains the structure determination of the (SO + 2O) phase on Cu(100) obtained by annealing an adsorbed SO_2 layer to about room temperature. Finally, a summary of the experimental structure determinations is given in section 10.

2. The geometric and electronic structure of gas-phase SO_2

Gas-phase SO_2 has an intramolecular S–O bond length of 1.43 Å [13] and the O–S–O angle measures 119° [14]. This results in an O–O distance of 2.48 Å as shown schematically in figure 1 (left). According to the point group C_{2v} the molecular orbitals (MOs) are labelled $a_1(\sigma)$, $a_2(\pi)$, $b_1(\pi)$ and $b_2(\sigma)$ with the corresponding symmetries given in brackets. The ground-state independent particle electron configuration together with the unoccupied valence orbitals may be written as [15, 16]

Core: $(1a_1)^2$ $\underbrace{(1b_2)^2\ (2a_1)^2}_{\text{O 1s}}$ $(3a_1)^2$ $\underbrace{(2b_2)^2\ (1b_1)^2\ (4a_1)^2}_{\text{S 2p}}$

S 1s S 2s

Valence: $(5a_1)^2\ (3b_2)^2\ (6a_1)^2\ (7a_1)^2\ (4b_2)^2\ (2b_1)^2\ (5b_2)^2\ (1a_2)^2\ (8a_1)^2$

Virtual MO: $(3b_1)^0\ (9a_1)^0\ (6b_2)^0$.

The latter antibonding virtual orbitals, which are probed in NEXAFS and inner-shell EELS (ISEELS), will be designated as b_1^*, a_1^* and b_2^* in the present work.

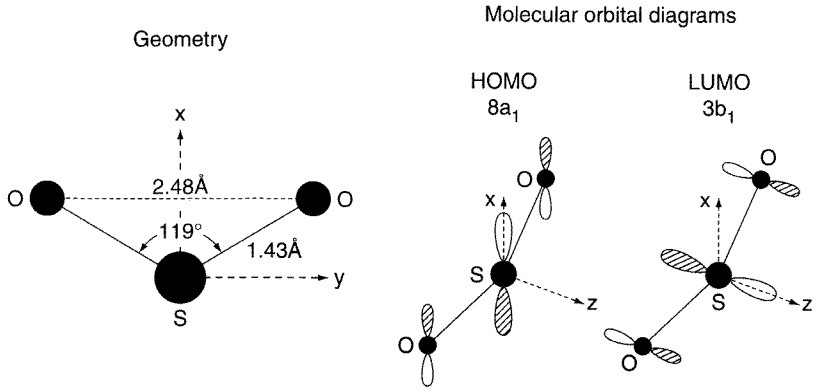

Figure 1. The geometric structure of gas-phase SO_2 and schematic diagrams for the highest occupied (HOMO) and lowest unoccupied (LUMO) molecular orbitals of SO_2, consisting mainly of p_x and p_z atomic orbitals, respectively. The molecular plane is defined as the x–y plane.

The most important orbitals from a bonding standpoint are the highest occupied MO (HOMO) $8a_1$ and the lowest unoccupied MO (LUMO) $3b_1 = b_1^*$. Both the HOMO and LUMO are mainly localized on sulphur [17] which suggests that bonding of SO_2 via the sulphur atom should predominate. Defining the molecular plane as the x–y plane with x lying along the twofold rotation axis, the HOMO consists of sulphur p_x (dominating) and s contributions and to a lesser extent of oxygen p_x, whereas the LUMO is formed by sulphur p_z and to a lesser extent oxygen p_z. The dominating p_x and p_z contributions are depicted in figure 1 (right). In transition metal–SO_2 complexes (see section 3) the bonding mechanism generally involves charge transfer from the HOMO of SO_2 into the orbitals of the complex fragments (σ donation) and charge transfer from the fragments into the LUMO of SO_2 (π back-donation) [3]. SO_2 thus exhibits a σ-donor and π-acceptor behaviour similar to that of CO [18]. Due to the higher electron affinity of SO_2 (1.1 eV [14]) compared to that of CO (-1.8 eV [19]) the LUMO of SO_2 is at lower energy, so its contribution to bonding is expected to be more important for SO_2 than for CO.

3. SO_2 coordination chemistry

Sulphur dioxide exhibits a rich coordination chemistry. In transition-metal complexes [3] SO_2 usually binds through its sulphur atom with a geometry which may be either planar or pyramidal or bridging as depicted in figure 2. In the η^1-planar binding configuration the metal (M), sulphur and both oxygen atoms are planar, while in the η^1-pyramidal geometry they are not. In addition, M–SO_2 configurations with SO_2 bonding through both sulphur and oxygen and through oxygen only (cf figure 2) have been identified. The intramolecular S–O bond length and the O–S–O angle of the complexes listed in [3] varies between 1.31 and 1.56 Å and between 108 and 119°, respectively. In general, the qualitative aspects of M–SO_2 bonding can be rationalized by just comparing the properties of the HOMO and LUMO of SO_2 with those of the valence orbitals of the relevant transition metal complex fragments [3]. Theoretical calculations [20] have shown that in a bond resulting from both σ donation and π back-donation the latter contribution dominates and is due to the high-lying transition metal d orbitals. The calculations also indicate that the binding energy

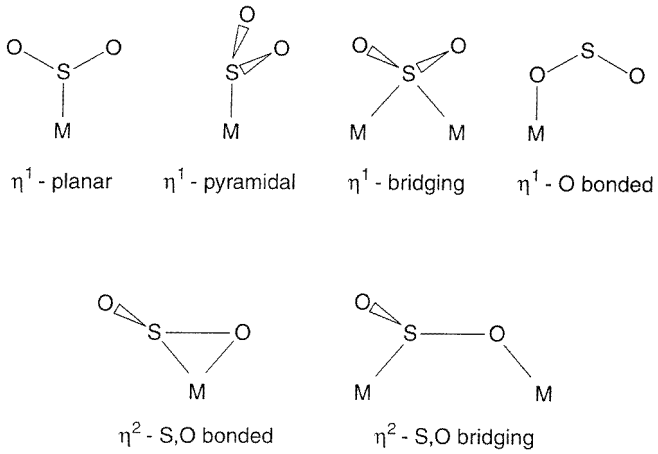

Figure 2. Typical coordination geometries for SO_2 in transition metal complexes. The superscript η notation refers to the number of atoms in SO_2 which are bonded to the metal.

gained by charge transfer from the metal into the LUMO of SO_2 increases in the order η^1-planar $< \eta^1$-pyramidal $< \eta^2$, so transition metal–SO_2 complexes should generally assume an η^1-pyramidal or η^2 configuration if not hindered by steric repulsion.

There is a correlation between the SO_2 coordination geometry and its vibrational (S–O stretching) frequencies, which has been summarized by Ryan *et al* [3] as depicted in figure 3. As can be seen from the figure, the symmetric (lower values) and asymmetric (higher values) S–O stretching frequencies of complexes with different M–SO_2 bonding configurations, ν_s and ν_a, respectively, lie in defined ranges, which partly overlap. This correlation can be valuable in diagnosing the coordination geometry of newly synthesized complexes and may help to determine the SO_2 bonding mode in surface complexes. In cases where the assignment on the basis of absolute values of stretching frequencies is not unambiguous, the difference $\nu_a - \nu_s$ can also be checked; this has values below 190 cm^{-1} for SO_2 bonding through S only, while values above 190 cm^{-1} indicate η^2-SO_2 configurations. As has been shown for CO and NO complexes [21], the surface-cluster analogy may, however, be misleading simply because the surface coordination modes are practically never the same as those in analogous ligand complexes.

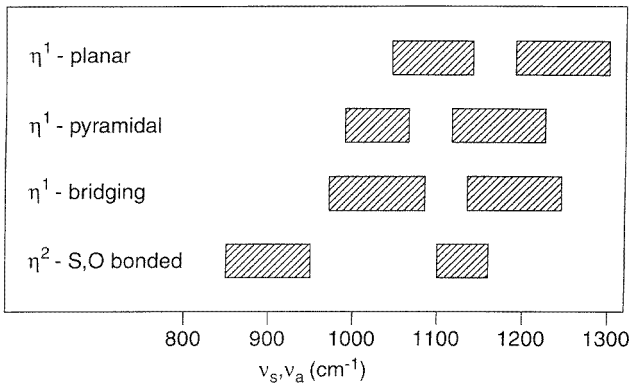

Figure 3. Symmetric (lower values) and asymmetric (higher values) S–O stretching frequencies for various SO_2 coordination geometries [3].

4. Temperature-dependent decomposition of adsorbed SO_2

Spontaneous or thermally activated decomposition of SO_2 has been reported on all metal substrates studied so far with one exception: on Ag surfaces SO_2 adsorbs and desorbs molecularly [8, 22–24]. Depending on temperature and initial SO_2 coverage different adsorbed decomposition products have been observed: SO species on Pt(111) [9, 25], Pd(100) [6] and Cu(100) [26, 27], SO_3 species on Cu(100)) [27] and SO_4 species on Pd(100) [6] and Pt(111) [9] in addition to atomic S and O. In most cases the identification of the adsorbed species ensued from EELS or HREELS measurements. Quite recently, SO_2 adsorption and temperature-dependent decomposition on Cu(100) [26] has been studied using fast and high-resolution XPS. The results of these experiments, performed at an advanced synchrotron radiation source (storage ring ELETTRA in Trieste, Italy), will be reported here. They not only allow the identification of adsorbed SO_x species, but also demonstrate the potential of this technique to study the kinetics of surface processes.

In figure 4 S 2p and O 1s XPS spectra are depicted taken during slow and continuous heating of the Cu(100) crystal initially dosed at 180 K with 5 L SO_2. It should be pointed out here that the shown curves correspond to single sweeps taken in a time of the order of 10 s. The S 2p data clearly show three different spin–orbit-split doublets located at binding energies ($p_{3/2}$ component of the doublet) of about 160.2, 164.3 and 165.3 eV. Initially the 164.3 eV doublet, which has been identified as SO_2 by NEXAFS [12], dominates. Upon heating to room temperature SO_2 disappears from the surface and the 165.3 eV doublet shows up together with the one at 160.2 eV. The latter can clearly be identified as atomic S by comparison with the spectrum measured on a Cu(100)–(2×2)–S reference structure. On the other hand, NEXAFS suggests an SO_x species with $x \neq 2$ for the 165.3 eV doublet. On further heating to about 390 K the SO_x species disappears nearly completely from the surface whereas the atomic S doublet hardly grows, but sharpens and slightly shifts in energy. Concerning different oxygen-containing species the O 1s data are less distinctive at first glance. Only one single peak, which shifts to lower binding energy on heating and initially broadens on increasing the temperature to about 273 K, is observed.

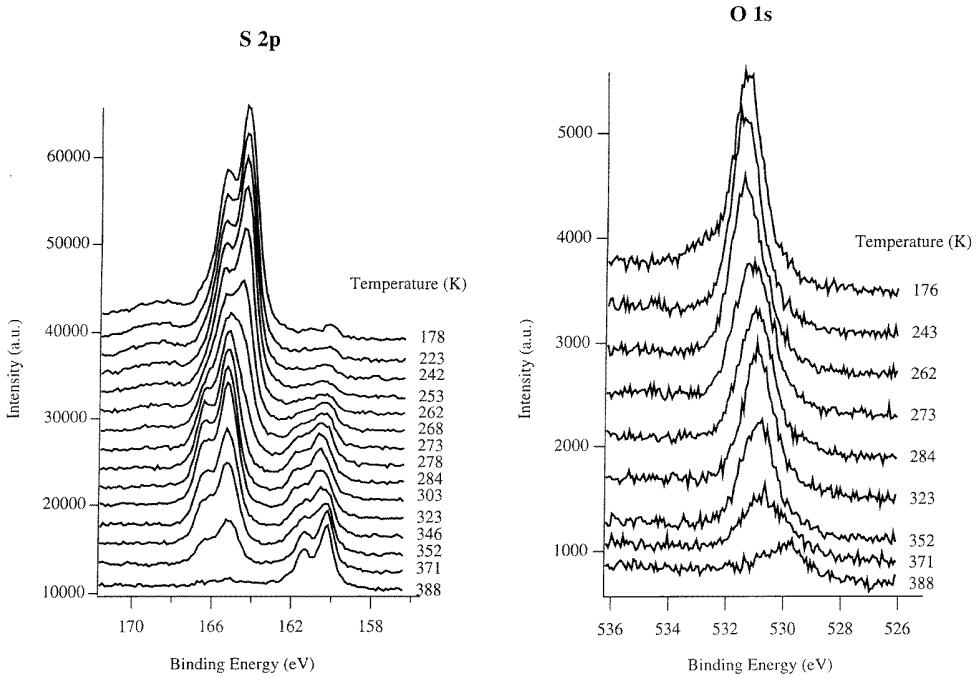

Figure 4. S 2p (left) and O 1s (right) core-level photoemission data for Cu(100)–SO_2 with the sample temperature as parameter during continuous heating ($\sim$0.1 K s^{-1}) [26].

In the first step of the analysis the individual S 2p and O 1s curves were fitted by assuming three main components each. In figure 5 the fits for four distinct temperatures are shown. As already discussed above, the three doublets used for the S 2p fits in figure 5 (left) are assigned to SO_2, SO_x ($x \neq 2$) and atomic S. As can be seen from the S 2p data, there is already partial dissociation (decomposition) on SO_2 adsorption at 180 K, indicated by small amounts of SO_x and atomic S. The O 1s data in figure 5 (right) are fitted with three main components located at 531.6, 530.9 and 530.2 eV. Within experimental accuracy the first one at 531.6 eV corresponds to both SO_2 (which dominates at 180 K) and SO_x

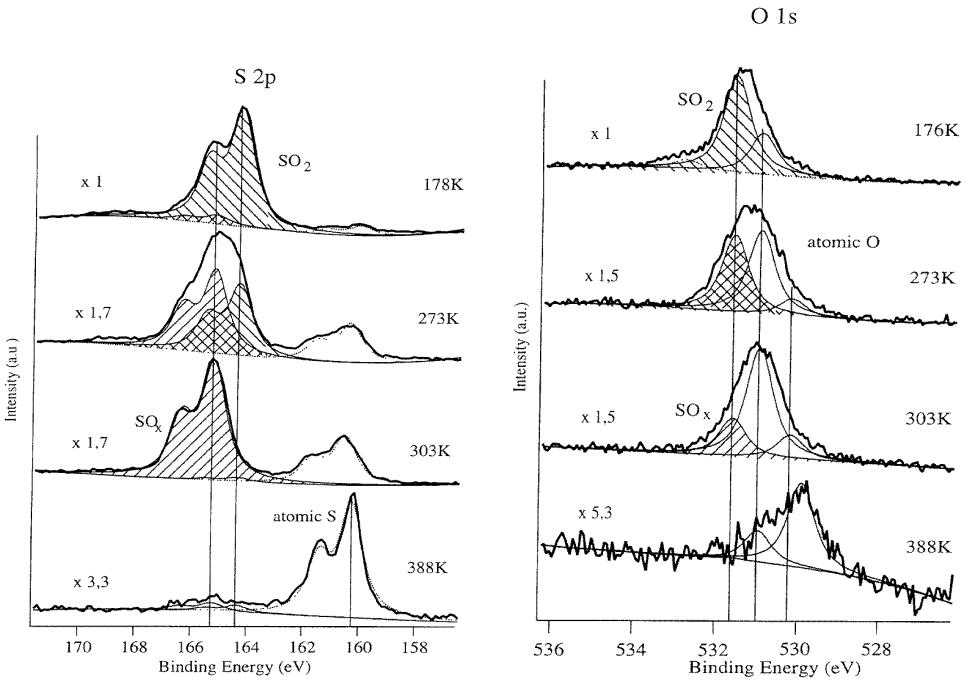

Figure 5. Curve fits of the S 2p (left) and O 1s (right) data of figure 4 for four distinct temperatures [26]. The S 2p spectra were fitted with three spin–orbit-split doublets located at 165.3 eV (SO_x), 164.3 eV (SO_2) and approximately 160.2 eV (atomic S). The O 1s data were fitted with three components located at 531.6 eV (SO_2 and SO_x), 530.9 eV (atomic O) and 530.2 eV (atomic O). The shifted atomic O component at ∼529.9 eV for 388 K is assigned to subsurface oxygen.

(which is exclusively present near room temperature), whereas the components at 530.9 and 530.2 eV are assigned to atomic oxygen in different adsorption sites. The dominant atomic oxygen contribution at room temperature has clearly been identified as oxygen in bridge sites by x-ray absorption [12]. The component at 530.2 eV might be oxygen in hollow sites, which are occupied on a clean Cu(100) surface [28]. Residual oxygen on the surface at temperatures of about 390 K and higher is assumed to be subsurface oxygen. The O 1s data also suggest partial dissociation (decomposition) on SO_2 adsorption at 180 K, indicated by the presence of atomic oxygen in the 176 K spectrum.

In order to identify the SO_x species the measured S 2p and O 1s intensities were calibrated with the corresponding intensities obtained for reference structures of known coverages, Cu(100)–(2×2)–S and Cu(100)–$(\sqrt{2} \times \sqrt{2})$R45°–O. The calibration results in an x value of 1.2 ± 0.4, which clearly identifies the SO_x species as SO. With the same calibration the ratio of the oxygen and sulphur coverages in the species dominating at the adsorption temperature measures 2.1 ± 0.2, showing that it is indeed SO_2 (as identified by NEXAFS).

According to the relatively large amount of atomic oxygen on the surface (cf figures 4 and 5) the following decomposition pathways are suggested:

$$SO_2 \rightarrow S(a) + 2O(a) \qquad SO_2 \rightarrow SO(a) + O(a).$$

It is interesting to note that upon SO_2 adsorption on Cu(100) at room temperature surface

SO_3 species in addition to SO have been observed [27]. This leads to the conclusion that the decomposition products SO(a) and O(a) react with SO_2 (room-temperature adsorption) to form SO_3:

$$SO(a) + SO_2(g) \rightarrow SO_3(a) + S(a) \qquad O(a) + SO_2(g) \rightarrow SO_3(a).$$

If, on the other hand, no SO_2 is delivered from the gas-phase environment during heating of adsorbed (at low temperature) SO_2, the decomposition product SO remains adsorbed on the surface until at more elevated temperature SO(a) and O(a) recombine and SO_2 is desorbed [26].

The formation of SO_4 on heating SO_2-covered Pd(100) and Pt(111) substrates to room temperature is assumed to be due to the following surface reaction [6, 9]:

$$SO_2(a) + 2O(a) \rightarrow SO_4(a).$$

This reaction can take place after the onset of SO_2 decomposition which supplies the required oxygen atoms.

5. SO_2 adsorption on Ag(110), Pd(100) and Pt(111): structural results

5.1. Ag(110)–SO_2

According to TPD [22–24], UPS and XPS [22], HREELS [8] and NEXAFS [7] measurements the scenario of SO_2 adsorption on Ag(110) can be summarized as follows.

Three different phases can clearly be distinguished as a function of temperature: multilayer, dual-layer and monolayer SO_2. After desorption of multilayers at about 120 K a second layer of SO_2 is quite stable up to about 140 K and desorbs at 175 K [22]. Above this temperature a single layer, which finally desorbs above 275 K, is observed. Annealing to temperatures $\geqslant$ 275 K restores the clean surface and thus shows that SO_2 desorbs completely and molecularly. The monolayer phase has been thoroughly investigated. The symmetric S–O stretching frequency measures 985 cm^{-1} compared to 1145 cm^{-1} in the gas phase, indicating a weakening of the S–O bond on adsorption due to the SO_2–Ag bond formation. This bond weakening was confirmed by the NEXAFS data as well as by theoretical calculations [17, 29]. The absolute value of $\nu_s = 985$ cm^{-1} indicates that SO_2 is bonded to Ag(110) only via the S atom (cf figure 3). Based on the presence of an SO_2–Ag out-of-plane bending (wagging) mode a tilted SO_2 geometry was suggested. This seems to be in conflict with the NEXAFS results, which showed that the plane of the SO_2 molecule was perpendicular to the surface and perpendicular to the close-packed $[1\bar{1}0]$ direction. The known experimental error of up to $\pm 15^\circ$ for an orientation determination using NEXAFS might, however, resolve this discrepancy. Quite recently the perpendicular orientation was confirmed by coverage-dependent NEXAFS experiments [30], which also showed that azimuthal ordering only occurs at low coverages. Based on the fact that the asymmetric stretch was not observed, an SO_2 adsorption geometry with the O–O axis parallel to the surface was suggested. Concerning the adsorption site, by making use of the surface-cluster analogy an on-top site was favoured [8]; this, finally, led to the qualitative structural model [7] depicted in figure 6.

MO–SCF calculations [17, 29] for η^1-planar and η^1-pyramidal SO_2 configurations in on-top sites on Ag(110) have confirmed the σ-donor and π-acceptor behaviour of SO_2 known from transition-metal complexes. They show that the SO_2–Ag(110) bond is primarily a consequence of the interactions of the HOMO and LUMO of SO_2 with the Ag(5s, 5p) orbitals. The 4d orbitals of Ag lie nearly 4 eV below the Fermi level [31], so they are too low in energy to supply charge into the LUMO of SO_2.

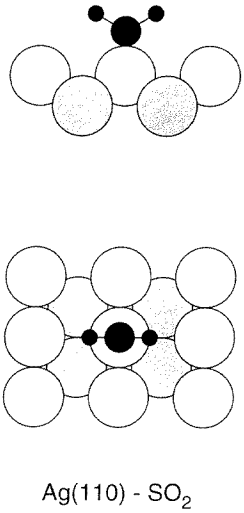

Figure 6. SO_2 adsorption geometry on Ag(110) deduced from NEXAFS and EELS measurements [7].

5.2. Pd(100)–SO_2

The adsorption of SO_2 on Pd(100) has been studied with TPD and EELS [6, 32]. According to these measurements SO_2 adsorbs intact on Pd(100) at temperatures below 120 K. Condensed multilayers of SO_2 desorb at 135 K, leaving a single layer on the surface, which on annealing to 190 K appears to order. Above 240 K decomposition of SO_2 occurs, yielding adsorbed SO and atomic oxygen on the surface. SO dissociates into S and O at higher temperatures. For initially high SO_2 coverages (multilayers) an SO_4 species is identified on the surface at about 300 K by reaction of SO_2 with oxygen which is supplied by SO_2 decomposition. SO_4 decomposes to S and O at higher temperatures. In the EEL spectra taken at 190 K both the symmetric and asymmetric stretching modes are observed, but no out-of-plane bending and no in-plane bending (rocking) modes. Based on the absence of the wagging mode a perpendicular orientation of the SO_2 molecular plane is suggested. Because ν_a is visible, the O–O axis cannot be parallel to the surface. SO_2 thus tilts in the plane of the molecule. Due to the absence of the rocking modes, the tilt is assumed to be slight. Although the measured symmetric ($\nu_s = 1035$ cm^{-1}) and asymmetric ($\nu_a = 1250$ cm^{-1}) stretching frequencies point to SO_2 bonding through S only (cf figure 3), the difference $\nu_a - \nu_s = 215$ cm^{-1} indicates 'some' Pd–O bonding, i.e. an η^2 SO_2 configuration. The proposed structural model is shown in figure 7.

As can be seen from the figure, the S atom is located in a fourfold hollow site and one oxygen atom close to a bridge site. This geometry (S and O sites) is suggested from the similarity of the EEL spectra for SO_2 adsorbed on Pd(100)–p(2 × 2)–S and on the clean surface.

Transferring the calculations of Sakaki *et al* [20] concerning SO_2 bonding in transition-metal complexes to surface complexes, an SO_2 configuration is expected in the latter which maximizes charge donation into the LUMO of SO_2 while minimizing steric repulsion. Quite generally, however, the metal substrate must have orbitals with the proper symmetry, energy and spatial extension to overlap with the LUMO. Ideal candidates for such a π-bond formation are metal d orbitals (cf section 3), which in the case of Pd extend to the Fermi level [31], so an η^2 configuration determined for Pd(100)–SO_2 is plausible.

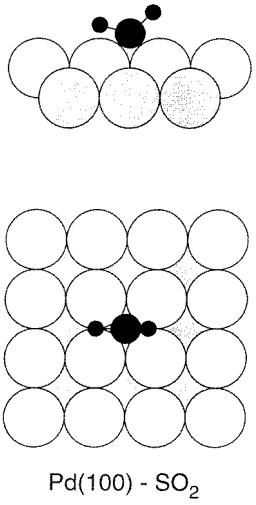

Figure 7. SO_2 adsorption geometry on Pd(100) deduced from EELS experiments [6].

5.3. Pt(111)–SO_2

Due to its role as catalyst poison the interaction of SO_2 with Pt surfaces at various temperatures has been of wide interest. The adsorption of SO_2 on Pt(111) has been studied with TPD [9, 25, 33, 34], Auger electron spectroscopy [35], work function change [34], UPS and XPS [9], as well as with HREELS [9]. According to these measurements [9] there is molecular adsorption at 120 K. Multilayers of SO_2 desorb around 130 K, leaving a single layer on the surface which finally desorbs at 285 K. After SO_2 adsorption at room temperature SO and SO_4 species are identified on the surface as in the Pd(100)–SO_2 system. It should be pointed out, however, that there is evidence of dissociative adsorption at 160 K for small SO_2 coverages [25, 34].

As in the case of Pd(100)–SO_2 the absence of the wagging mode in the HREEL spectra suggests a perpendicular orientation of the molecular plane. The measured symmetric ($\nu_s = 940$ cm^{-1}) and asymmetric ($\nu_a = 1252$ cm^{-1}) S–O stretching frequencies and, especially, the difference $\nu_a - \nu_s = 312$ cm^{-1} point to an η^2 configuration with SO_2 bonding to Pt through its S and one O atom. O bonding is supported by the presence of a Pt–O loss feature. By comparing the intensity ratio, ν_a/ν_s, with that measured for Pd(100)–SO_2, a larger in-plane tilt for SO_2 on Pt(111) than on Pd(100) is suggested.

The most likely site for SO_2 adsorption on Pt(111) is guessed by an MO analysis [9]. With the Pt d band extending in energy up to the Fermi level [31], strong π bonds should be formed by charge transfer from the d orbitals into the LUMO of SO_2, in agreement with the UPS and XPS results. The MO analysis favours an adsorption site with one S–O bond bridging two Pt atoms as depicted schematically in figure 8. As can be seen from the figure, this geometry yields maximum overlap of the Pt d_{xz} or d_{yz} orbitals with the LUMO of SO_2 (on the left) forming a π bond. In addition, a σ bond is also possible by charge transfer from the HOMO of SO_2 into Pt d_z^2 orbitals (on the right).

A complete understanding of the bonding of SO_2 to Ag(110), Pd(100) and Pt(111) discussed in this section and to metal surfaces in general is, however, only possible by theoretical calculations for SO_2 in its various configurations and adsorption sites.

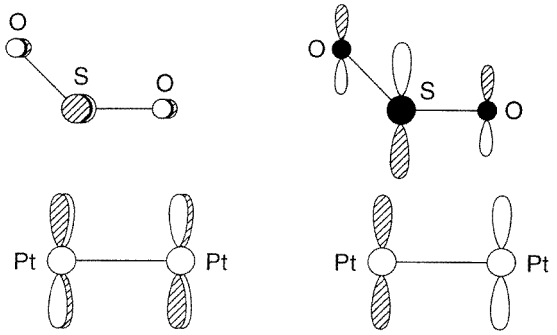

Figure 8. A possible SO_2 adsorption geometry on Pt(111) deduced from HREELS and MO analyses [9].

A final question which needs to be addressed concerns the different adsorption and desorption behaviour of SO_2 on Ag(110) compared to Pd(100) and Pt(111). As has been shown in this section, SO_2 desorbs completely and molecularly from Ag(110), while it decomposes on Pd(100) and Pt(111) upon heating to room temperature. One might argue that due to participation of the O atoms in bonding of SO_2 with Pd(100) and Pt(111) a stronger SO_2–metal bond, which leads to more facile dissociation, is formed. This, however, does not seem to be true. As can be seen from a comparison of the symmetric S–O stretching frequency for SO_2 on Ag(110) ($\nu_s = 985$ cm^{-1}) to that on Pd(100) ($\nu_s = 1035$ cm^{-1}), SO_2 adsorption on Ag(110) results in an even greater weakening of the S–O bond compared to that on Pd(100). We can only speculate that for SO_2 on Ag(110) the activation energy for dissociation is larger than that for SO_2 adsorbed on Pd(100), which means that the participation of the more directional d orbitals in bonding leads to a lowering of the activation energy for dissociation. We should, however, always bear in mind that the surface-cluster analogy may be misleading (cf section 3). For all the systems discussed in this section quantitative structure determinations are therefore desired.

6. SEXAFS and NEXAFS formalism

The quantitative structure determinations of condensed SO_2 multilayers, of SO_2 adsorption on Ni(110), Ni(100), Ni(111) and Cu(100) presented in sections 7–9 were performed by use of XAFS measurements. This section, therefore, includes a brief review of the SEXAFS and NEXAFS formalism to give the reader the possibility of assessing the reliability of the results reported in sections 7–9.

6.1. SEXAFS

The oscillatory part of the absorption coefficient $\mu - \mu_0$ beyond some 10 eV above the edge (cf figure 10), normalized to the structureless background μ_0, results from the interference between the emitted photoelectron wave and the waves backscattered from neighbouring atoms. For K and L_1 edges it is given by [36]

$$\chi(k) = \frac{\mu - \mu_0}{\mu_0} = -\sum_i A_i(k)\ \sin[2kR_i + \psi_i(k)] \tag{1}$$

where the summation extends over all neighbouring shells i of atoms separated from the absorbing atom by the same distance R_i, A_i is the amplitude, $\psi_i(k)$ is the phase shift and the photoelectron wave number k is related to the photon energy E by

$$k = \hbar^{-1}[2m(E - E_0)]^{1/2} \tag{2}$$

where $\hbar$ is Planck's constant, m is the electron mass and E_0 is the threshold energy and corresponds to the zero of the photoelectron kinetic energy scale.

A Fourier transform of $\chi(k)$ reveals the different absorber–back-scatterer distances R_i, which, however, can only be calculated if the phase shifts $\psi_i(k)$ are known. Phase shifts for a particular pair of absorbing and back-scattering atoms can be either calculated or transferred [37] from a suitable model compound to the system under investigation.

The information on the positions of adsorbed atoms and molecules, the adsorption site, is contained in the SEXAFS amplitude

$$A_i(k) = \frac{N_i^*}{kR_i^2} F_i(k) \exp[-2\sigma_i^2 k^2] \exp\left[-\frac{2R_i}{\lambda_i(k)}\right] \tag{3}$$

which includes the polarization-dependent effective coordination number N_i^*

$$N_i^* = 3\sum_j^{N_i} \cos^2 \alpha_{ij} \qquad \alpha_{ij} = \measuredangle(\boldsymbol{E}, \boldsymbol{r}_{ij}) \tag{4}$$

where α_{ij} is the angle between the vector $\boldsymbol{E}$ of the incoming radiation at the absorbing atom site and the vector $\boldsymbol{r}_{ij}$ from the absorbing atom to the jth atom in the ith shell. $F_i(k)$ is the back-scattering amplitude of the neighbouring atoms and exponential terms $\exp[-2\sigma_i^2 k^2]$ and $\exp[-2R_i/\lambda_i(k)]$ account for vibrational effects and inelastic scattering of the photoelectrons with a mean free path $\lambda_i(k)$, respectively.

Owing to the $\cos^2\alpha$ dependence of the effective coordination number all neighbours located in a certain direction relative to the absorbing atom are revealed by varying the $\boldsymbol{E}$ vector orientation. High-symmetry adsorption sites can therefore be determined easily by polarization-dependent measurements. According to (3) and (4) the ratio of first-neighbour SEXAFS amplitudes A_1 determined for the same sample at different angles of x-ray incidence θ_i is equal to the ratio of the corresponding effective coordination numbers N_1^*

$$A_1(\theta_1)/A_1(\theta_2) = N_1^*(\theta_1)/N_1^*(\theta_2). \tag{5}$$

The measured amplitude ratio is generally sufficient to distinguish between different high-symmetry sites. For more complicated systems the SEXAFS function $\chi(k)$ calculated for model structures using (1)–(4) must be compared with polarization-dependent experimental $\chi(k)$ functions in a trial and error procedure.

It must be emphasized that SEXAFS is a very local probe, not requiring long-range order as in conventional LEED. It is clear from (1) and (3) that SEXAFS spectra are dominated by a small number (often only one or two) of near-neighbour shells of atoms.

6.2. NEXAFS

The structure in the near-edge range of molecular absorption spectra is dominated by the excitation of core electrons into unfilled antibonding orbitals of π and σ symmetry. The orientation determination by means of the polarization dependence of NEXAFS data follows directly from the matrix element for an electronic transition in a molecule [38]. The absorption intensity is given by

$$I \propto |\boldsymbol{E} \cdot \langle f|\boldsymbol{M}|i\rangle|^2 \tag{6}$$

where $\boldsymbol{M}$ is the electric-dipole vector associated with the transition. For $I \neq 0$ the product of the irreducible representations corresponding to $|f\rangle$, $|i\rangle$ and $\boldsymbol{M}$ must be totally symmetric, or at least contain the totally symmetric representation. For the π and σ resonances of an oriented diatomic molecule (with z parallel to the molecular axis) at a K edge the angular dependence is given by

$$I_\pi \propto |\boldsymbol{E} \cdot \boldsymbol{M}_{xy}(\pi)|^2 \propto \sin^2 \beta \tag{7}$$

$$I_\sigma \propto |\boldsymbol{E} \cdot \boldsymbol{M}_{z}(\sigma)|^2 \propto \cos^2 \beta \tag{8}$$

where β is the angle between the electric vector and the molecular axis. If the molecule is tilted or lies flat on the surface, then the point-group symmetry is lowered, the degeneracy of the π orbitals is lifted, and the simple equations (7) and (8) are no longer valid. In most cases studied so far, however, it is possible to treat the adsorbed molecule simply as an oriented species and to neglect the interaction with the substrate.

For low-Z diatomic molecules or pseudo-diatomics there is a strong correlation between σ resonance position and intramolecular bond length [39], which allows an absolute determination of the latter. In all other cases changes in intramolecular bond lengths upon adsorption can at least be measured.

7. Condensed mutlilayers of SO_2

The NEXAFS of condensed SO_2 multilayers taken above the S K edge at the storage ring BESSY in Berlin behind the double-crystal monochromator KMC [40] is shown in figure 9 (bottom) together with the corresponding gas-phase data [41]. The spectra are rather similar and dominated by transitions into the antibonding b_1^* (designated as π^* in the present work) and $a_1^* + b_2^*$ (designated as σ^*) molecular orbitals. The a_1^* and b_2^* resonances are not resolved, but, due to the better resolution in the gas-phase experiment, an energy separation of 0.5 eV can be estimated in comparison to 0.76 eV determined with ISEELS [16]. It should be pointed out that the Rydberg transitions, designated as R in the gas-phase spectrum, are quenched in the solid. The nearly identical (within experimental accuracy) energy positions of the π^* and σ^* resonances in gas-phase and condensed SO_2 suggest a nearly identical intramolecular S–O bond length. This was checked with SEXAFS measurements.

In figure 10 O K-edge (S)EXAFS raw data (left) of gaseous (top) and condensed (bottom) SO_2 [42] are shown together with the corresponding background-subtracted $\chi(k)$ functions multiplied by k (middle) and their Fourier transforms (right). The background-subtracted data and the Fourier transforms are again rather similar. In particular, the dominating Fourier peak corresponding to the intramolecular O–S distance is located at exactly the same position in r, which means that within experimental accuracy of ± 0.02 Å the intramolecular bond length in gaseous and condensed SO_2 is identical (1.43 Å). Minor differences in the width of the O–S Fourier peak and in the additional structure of the Fourier transform are due to the increased vibrations in the gas phase compared to the solid and to the presence of higher-neighbour O–S distances in the solid, respectively.

8. SO_2 adsorption on Ni(110), Ni(100) and Ni(111)

8.1. Ni(110)–SO_2

According to a TPD, XPS and ARUPS study [4], SO_2 adsorption on Ni(110) at temperatures below 100 K is associative. On exposing the surface to large amounts of SO_2 condensed

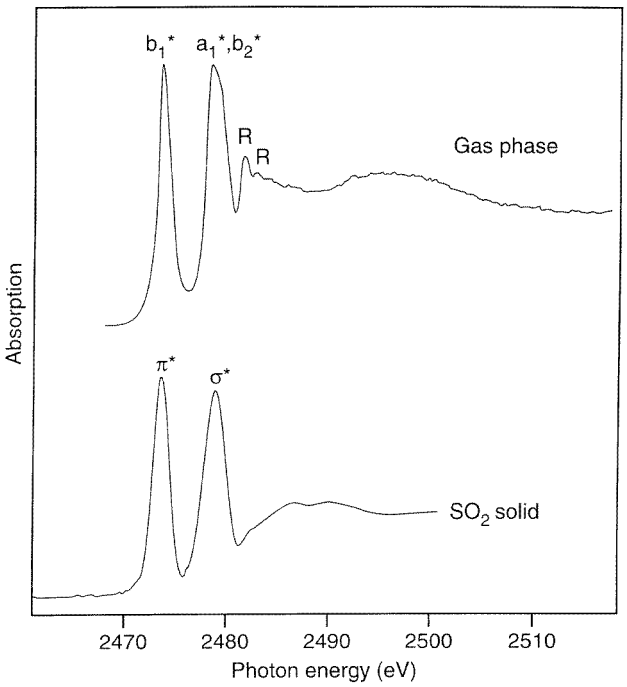

Figure 9. Sulphur K edge NEXAFS spectra of gas-phase [41] and condensed SO_2. Rydberg transitions are designated as R.

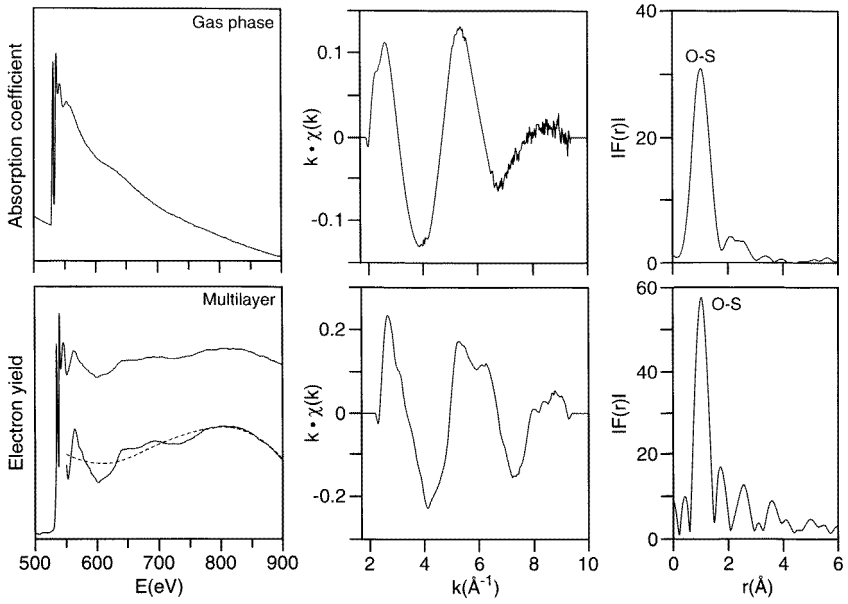

Figure 10. Left, oxygen K-edge EXAFS spectra of gaseous SO_2 (top) and of SO_2 condensed on Cu(100) (bottom) together with the spline-polynomial background (dashed line) fitted to the (enlarged) signal. Middle, background-subtracted data converted into the k scale and multiplied by k. Right, Fourier transforms of the background-subtracted data [42].

multilayers, which desorb at about 130 K, are formed. The remaining SO_2 monolayers desorb at 360 K, leaving large amounts of atomic S on the surface. This was taken as evidence for SO_2 decomposition upon heating into atomic sulphur and oxygen. The saturated chemisorbed layer, which exhibits a c(2×2) LEED pattern, was assigned to a coverage of 0.5 ML by XPS and differences in the relative peak intensities of the spin–orbit-split S 2p doublet for the saturated and the low-coverage (0.15 ML) phase were not attributed to SO_x species with $x \neq 2$. We should point out, however, that the XPS spectrum of the saturated layer clearly exhibits atomic S features indicative of SO_2 decomposition. The ARUPS results for the low-coverage phase suggest an orientation of the molecular plane perpendicular to the surface and perpendicular to the close-packed [$1\bar{1}0$] rows with an in-plane tilt allowing SO_2 bonding to the substrate also via the O atom as found for Pd(100) and Pt(111) surfaces.

We now focus on a recent surface structure determination of the low-coverage SO_2 phase on Ni(110) by use of XAFS [11]. In this study SO_2 was adsorbed at 170 K, resulting in submonolayer coverages of about 0.2 ML. The NEXAFS data taken above the S K-edge at different polar angles θ in both the $\langle 110 \rangle$ and $\langle 100 \rangle$ azimuths are shown in figure 11 (middle and bottom respectively) together with the multilayer NEXAFS spectrum (top). The polarization dependence of the π^* and σ^* resonances in both azimuths with σ^*-resonance intensities being largest at normal ($\theta = 90^\circ$) and π^*-resonance intensities dominating at near-grazing ($\theta = 15^\circ$) x-ray incidence immediately suggests SO_2 species with molecular planes oriented approximately parallel to the surface. A quantitative intensity analysis of the σ^* and π^* resonances yields a tilt angle with respect to the surface normal of $90 \pm 10^\circ$ [46]. We should point out, however, that the NEXAFS structure at about 2480 eV might indicate another SO_x species with $x \neq 2$ present on the surface. From the shift of the σ^* resonance position towards lower energies compared to that in solid SO_2 (cf figure 11) an increase of the intramolecular bond length, which can be quantified by SEXAFS measurements, is suggested [39].

The Fourier transforms of background-subtracted S K-edge SEXAFS data taken at different polar angles θ in both the $\langle 110 \rangle$ and $\langle 100 \rangle$ azimuths are depicted in figure 12. They are dominated by two peaks which correspond to the S–O (SO_2) and nearest-neighbour (nn) S–Ni distances. According to (3) and (4) the polarization dependence of the S–O peak in both azimuths immediately suggests nearly flat-lying SO_2 molecules, in agreement with NEXAFS. An average S–O bond length of 1.49 ± 0.03 Å was calculated, indicating an intromolecular bond weakening as a result of the adsorbate–substrate bond formation which is in qualitative agreement with the NEXAFS result. While the amplitude of the S–O Fourier peak located close to 1 Å might suffer from background-subtraction problems, the amplitudes of the S–Ni peaks can be used to accurately determine the adsorption site of the S atoms according to (5). In table 1 calculated ratios of effective coordination numbers for hollow, long-bridge, short-bridge, on-top and a 1:1 mixture of long-bridge and short-bridge adsorption sites, assuming the measured average nn S–Ni bond length of 2.20 ± 0.03 Å, are listed and compared with experimental amplitude ratios. As can be seen from the table, all simple high-symmetry sites can safely be excluded, while a structure with 50% of the S atoms in long-bridge and 50% in short-bridge sites can perfectly reproduce the experimental result within an estimated accuracy of $\pm$10–15%. Consequently, the schematic structural model shown in figure 13 was suggested. Assuming an S–Ni distance of 2.20 Å, an intramolecular S–O bond length of 1.49 Å and an O–S–O bond angle of 119° (as in the gas phase), flat-lying SO_2 molecules as depicted in the figure would exhibit nn O–Ni distances of 2.11 and 2.28 Å in long- and short-bridge adsorption sites, respectively. Tilts of the molecular plane of the order of 20° with respect to the surface can, however, easily

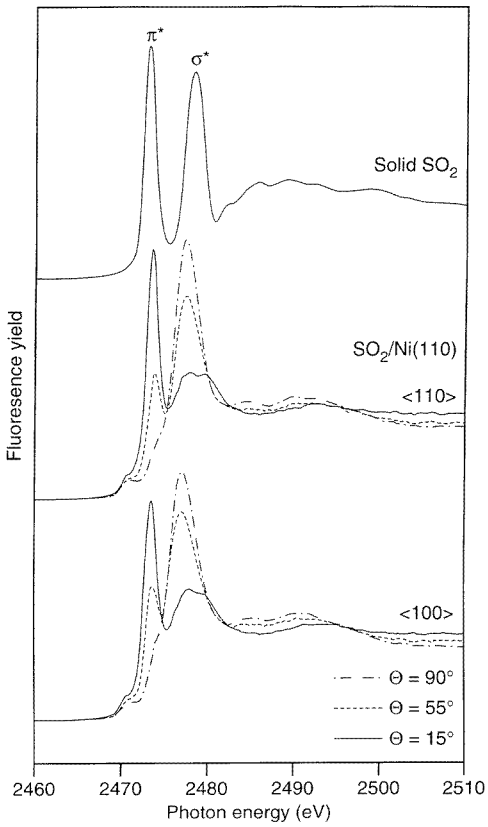

Figure 11. Sulphur K-edge spectra of condensed SO_2 (top) and SO_2 adsorbed on Ni(110) taken at different polar angles θ in both the $\langle 110 \rangle$ (middle) and $\langle 100 \rangle$ (bottom) azimuths [11].

change these numbers by ± 0.2 Å. Oxygen K-edge SEXAFS measurements are, therefore, very necessary to determine the correct location of the oxygen atoms.

Our own XAFS and XPS measurements [43] on the saturated layer confirm the above results concerning an approximately flat-lying geometry with S atoms in long- and short-bridge sites, but they also unambiguously show that the NEXAFS structure at about 2480 eV (cf figure 11) is due to adsorbed SO_3 species (a_1^* resonance), which after heating the saturated layer to about room temperature are the only SO_x species adsorbed on the surface. Increased amounts of SO_3 in the saturated layer compared to the low-coverage phase are also responsible for the changed relative intensities of the spin–orbit-split S 2p doublet in the XPS of those two phases (cf figure 2 in [4]). Two conclusions can be drawn from these results: (i) adsorption of SO_2 at temperatures around 170 K is partly dissociative; SO_3 species are formed on adsorption as well as after heating SO_2 layers to room temperature; (ii) the σ^* resonance is not an ideal candidate for an orientation determination in the present system. Both the a_1^* and e^* resonances of SO_3 overlap with the σ^* resonance of SO_2. Moreover, due to the different polarization dependences of the a_1^* and b_2^* components forming the σ^* resonance [7] complications arise in general if the molecule is not flat lying.

Although atomic S adsorbs in hollow sites on Ni(110) [44], SO_2 adsorption in bridge sites is not unreasonable if additional bonding through the O atoms occurs. Obviously, the roughly planar geometry of SO_2 on Ni(110) with S atoms in bridge sites maximizes charge

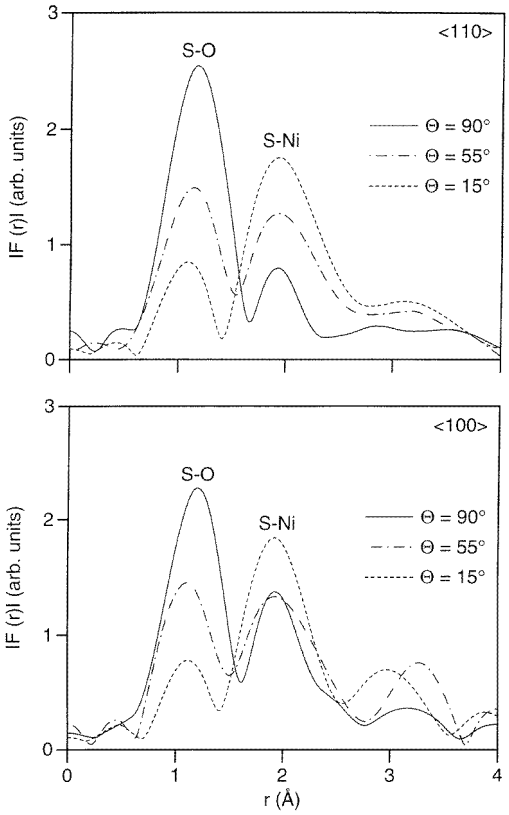

Figure 12. Fourier transforms of the background-subtracted SEXAFS data of Ni(110)–SO_2 taken at different polar angles θ in both the ⟨110⟩ (top) and ⟨100⟩ (bottom) azimuths [11].

Table 1. Experimental and theoretical amplitude ratios $A(\theta,$ azimuth$)/A(\theta = 15^\circ, \langle 110\rangle)$ calculated for twofold hollow, long-bridge, short-bridge, on-top and a 1:1 mixture of long- and short-bridge (ℓ + s) sites assuming an S–Ni distance of 2.20 Å.

		Amplitude ratio					
			Calculation				
Azimuth	$\theta(^\circ)$	Exp	Hollow	Long bridge	Short bridge	on-top	ℓ + s bridge
⟨110⟩	15	1.00	1.00	1.00	1.00	1.00	1.00
	55	0.65	1.11	0.39	0.67	0.35	0.58
	90	0.33	1.17	0.06	0.49	0	0.34
⟨100⟩	15	1.01	1.07	1.12	0.97	1.00	1.02
	55	0.80	1.83	1.63	0.35	0.35	0.79
	90	0.66	2.24	1.91	0.02	0	0.66

donation into the LUMO (π^*) of SO_2 with no steric hindrance (cf subsection 5.2). Due to steric repulsion flat-lying SO_2 molecules with S atoms in hollow sites, on the other hand, must be excluded.

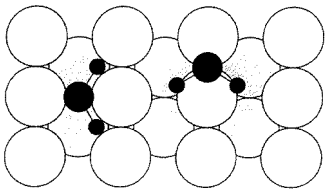

Figure 13. SO_2 adsorption geometries on Ni(110) deduced from XAFS measurements [11].

The orientation of the molecular plane parallel to the surface as determined with XAFS is in conflict with the ARUPS study [4], which by using symmetry selection rules suggests upright-standing molecules. Although the authors of [4] cannot completely rule out a planar geometry, the comparison, nevertheless, shows how easily qualitative techniques may fail.

8.2. Ni(111)–SO_2 and Ni(100)–SO_2

Sulphur K-edge NEXAFS and SEXAFS measurements as described in the previous section have also been conducted on SO_2 adsorption on Ni(111) and Ni(100) [10] at 170 K. The data correspond to coverages of about 0.4 ML.

The NEXAFS spectra of Ni(111)–SO_2 and Ni(100)–SO_2 are qualitatively rather similar and exhibit the same polarization dependence as those shown in figure 11 for Ni(110)–SO_2. From the qualitative intensity analyses of both the π^* and σ^* resonances [46] a flat-lying geometry is suggested as on Ni(110). Shifts of the σ^*-resonance energy to lower values compared to those in the multilayer NEXAFS indicate a weakening of the intromolecular bond on adsorption. The SEXAFS data confirm flat-lying SO_2 species and yield intramolecular S–O bond lengths of 1.48 and 1.51 Å for Ni(111) and Ni(100), respectively, compared to 1.43 Å for gas-phase and condensed SO_2. The nn S–Ni distances measure 2.16 ± 0.03 Å and 2.18 ± 0.03 Å on Ni(111) and Ni(100), respectively, and are approximately equal to the S–Ni bond lengths of adsorbed atomic S on the corresponding Ni surfaces. From the SEXAFS amplitude analyses sulphur locations in bridge sites on both Ni(111) and Ni(100) can be concluded in contrast to the hollow-site adsorption of atomic S on these surfaces. Obviously, the same arguments concerning maximum orbital overlap and steric hindrance as for SO_2 adsorption on Ni(110) apply. Schematic structure models deduced from XAFS are shown in figure 14. Assuming the measured S–Ni and S–O distances, SO_2 configurations as depicted in this figure would result in average nn O–Ni distances of about 2.2 Å on both surfaces,. Oxygen K-edge SEXAFS measurements are, however, very necessary to determine the correct location of the oxygen atoms.

We should point out here that the S K-edge NEXAFS spectra of Ni(111)–SO_2 and Ni(100)–SO_2 exhibit a similar structure at about 2480 eV as that of Ni(110)–SO_2, which for the latter can be assigned to adsorbed SO_3. It can thus be concluded that SO_2 adsorption on Ni(111) and Ni(100) at 170 K is partly dissociative.

9. SO_2 adsorption on Cu(100)—surface structure determination of Cu(100)–(SO + 2O)

As can be seen from a TPD and XPS study [26], SO_2 adsorption on Cu(100) at 180 K is partly dissociative. In addition to 0.25 ML SO_2, small amounts of SO and atomic S as well as larger amounts of atomic O are observed on the surface (cf figures 4 and 5). Below

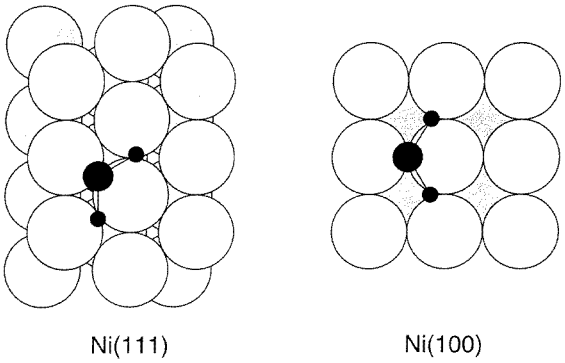

Figure 14. SO_2 adsorption geometries on Ni(111) (left) and Ni(100) (right) deduced from XAFS measurements [10].

room temperature SO_2 partly desorbs and partly decomposes, leaving increased amounts of SO, atomic S and atomic O on the surface exhibiting a weak (2×2) LEED pattern. Below 400 K SO + O recombine to form SO_2, which desorbs from the surface. The only species detected on the surface at higher temperatures are atomic S and atomic O (subsurface).

An XAFS study [12] indicates upright-standing SO_2 molecules on adsorption at 180 K. The data are, however, not consistent with a single adsorption geometry. SO_2 is bonded to Cu(100) through at least one oxygen atom with an O–Cu distance of about 2.0 Å in addition to bonding through S with an S–Cu distance of about 2.3 Å. The intramolecular S–O bond is lengthened on adsorption and there seems to be some evidence for two different S–O bond lengths within the same SO_2 molecule. Co-adsorbed atomic oxygen is located in bridge sites.

We now focus on the structure determination of the (SO + 2O) phase obtained after heating a condensed SO_2 layer to about room temperature. This study [12] involves a combined S and O K-edge SEXAFS analysis.

Background-subtracted sulphur and oxygen K-edge SEXAFS data of (SO + 2O) taken at normal (top) and near-grazing (bottom) incidence together with the corresponding Fourier transforms (dashed lines) are depicted in figures 15 and 16, respectively. The poor statistics of the sulphur K-edge data is due to the relatively low photon flux at BESSY around 2.5 keV and higher. As can be seen from figures 15 and 16, the Fourier transforms consist of intramolecular (O–S, S–O) and adsorbate–substrate (O–Cu, S–Cu) peaks. Neither the oxygen nor the sulphur data taken at $\theta = 20^\circ$ show an intramolecular Fourier peak. According to (3) and (4) this indicates flat-lying SO species.

The Fourier analysis of the sulphur data yields an nn S–Cu distance of 2.36 ± 0.05 Å and an amplitude ratio of $A(90^\circ)/A(20^\circ) = 0.76 \pm 30\%$ for this peak. A comparison of this experimental amplitude ratio with calculated values for a hollow site (0.75), a bridge site (0.23) and for on-top adsorption (0) clearly suggests SO adsorption with S atoms occupying fourfold hollow sites. This also holds when we take into account the increased amount of atomic sulphur on the surface (see figures 4 and 5) which is known to adsorb in fourfold hollow sites on clean Cu(100) [45]. A comparison of the measured S–Cu bond length of 2.36 ± 0.02 Å with that for atomic S on clean Cu(100) 2.27 ± 0.02 Å [45], indicates strong bonding of the SO species to the surface through the S atom. We should mention here that the poor fit of the S–O Fourier peak in the transform of the 90° data in figure 15 is attributed to the less reliable theoretical S–O phase shift used in the analysis.

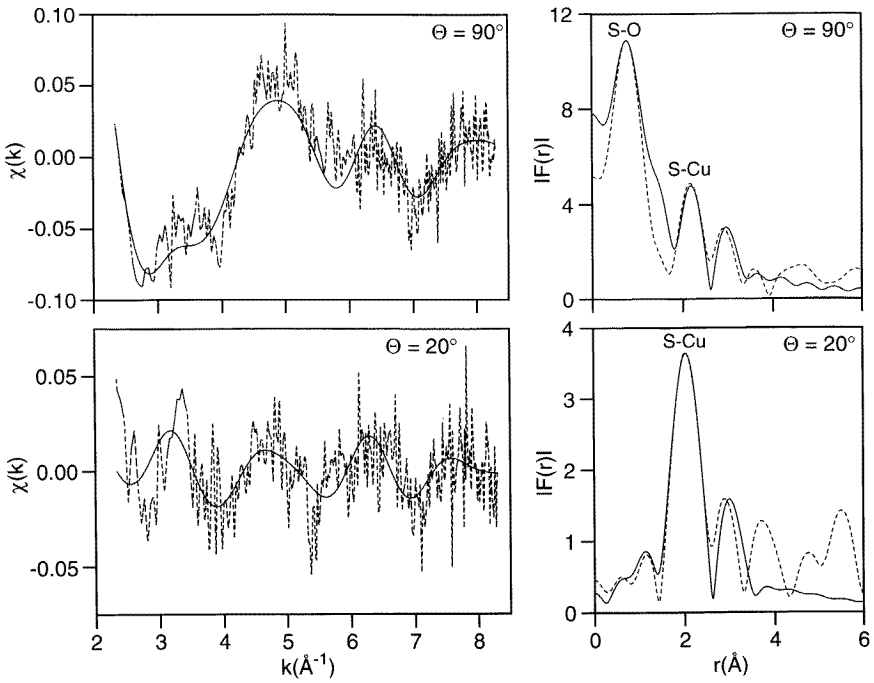

Figure 15. Background-subtracted sulphur K-edge SEXAFS spectra (left, dashed lines) of the phase formed by heating a condensed SO_2 multilayer to 280 K and their Fourier transforms (right, dashed lines) compared with SEXAFS simulations (solid lines) for normal (top) and near-grazing (bottom) x-ray incidence, assuming flat-lying SO species with S atoms located in hollow sites [12].

The Fourier analysis of the oxygen K-edge data yields an intramolecular O–S bond length of 1.41 ± 0.03 Å and an O–Cu distance of about 1.95 Å, which according to the XPS results (figure 5), must be due to an 'average' of the O–Cu distance from SO and that from co-adsorbed atomic oxygen. The much larger amplitude of the O–Cu Fourier peak for $\theta = 20^\circ$ compared to that for $\theta = 90^\circ$ immediately suggests oxygen positions close to bridge sites rather than in hollow sites. We therefore simulated our data using the structural model shown in figure 17. The SO species are lying flat on the surface in [001] or [$0\bar{1}1$] direction (two domains) with S atoms occupying fourfold hollow sites and O atoms nearly bridging two substrate Cu atoms. Co-adsorbed atomic oxygen is located in bridge sites. The structural parameters used for the best fit (solid lines) in figure 16 are: $R_{\mathrm{S–Cu}} = 2.34 \pm 0.05$ Å, $R_{\mathrm{O–S}} = 1.41 \pm 0.03$ Å, $R_{\mathrm{O–Cu}}(\mathrm{SO}) = 1.93 \pm 0.05$ Å, $R_{\mathrm{O–Cu}}(\text{atomic O}) = 1.96 \pm 0.05$ Å. The S–Cu bond length calculated from the O K-edge data is in good agreement with the value obtained from the S K edge. The measured O–Cu bond lengths are close to the value of 1.86 ± 0.03 Å found for atomic oxygen adsorbed in hollow sites on clean Cu(100) [28], indicating strong bonding of the SO species to the surface also through the O atom. The additional peak B in the $\theta = 90^\circ$ Fourier transform is due to next-nearest neighbours from oxygen atoms located in bridge sites. It cannot be reproduced by atomic O in hollow sites. Transformations with an upper limit of $k \sim 8$ Å^{-1} show that the slight misfit of peak B is the result of the 'irregularity' in the experimental spectrum around $k \sim 8$ Å^{-1}. As can be seen from the single-shell analysis in figure 16 (right) the amount of atomic oxygen used in

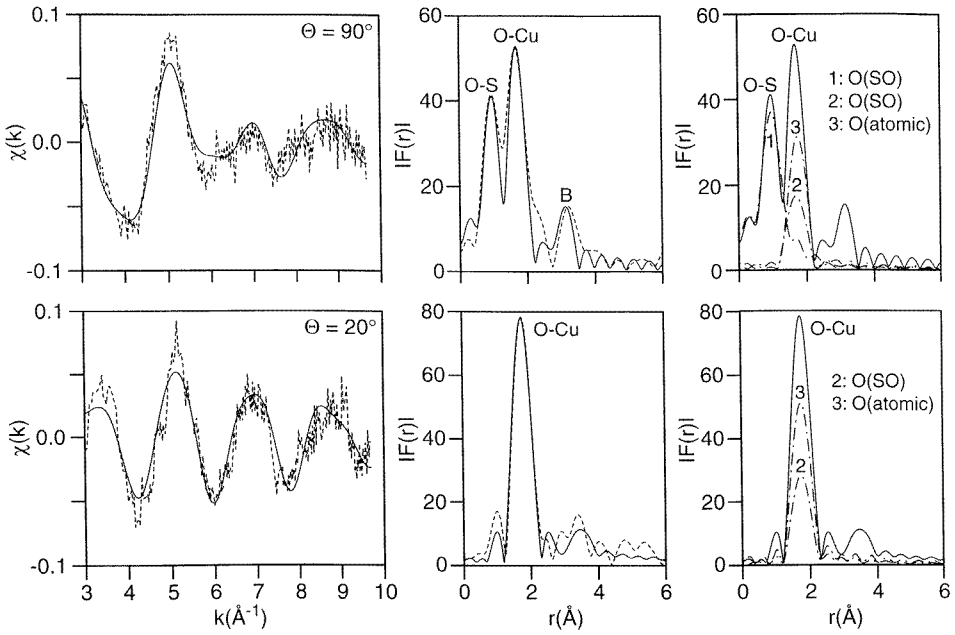

Figure 16. Background-subtracted oxygen K-edge SEXAFS spectra (left, dashed lines) of the phase formed by heating a condensed SO_2 multilayer to 280 K and their Fourier transforms (middle, dashed lines) compared with SEXAFS simulations (solid lines) for normal (top) and near-grazing (bottom) x-ray incidence, assuming the local geometry of figure 17. In the right-hand panels the single-shell contributions (dash–dotted lines) to the overall simulations (solid lines) are shown [12].

the simulation (best fit) is exactly twice the amount of oxygen in the SO species, in good agreement with the XPS results of figure 5. This also means that on the real surface there must be areas with more atomic oxygen and less SO compared to the (2×2)–$(SO + O)$ structure shown in figure 17, and also some atomic sulphur. The negligible amount of a second atomic oxygen species seen with XPS is assigned to oxygen atoms adsorbed in hollow sites.

We should emphasize here that the 'construction' of the structural model for $(SO + 2O)$ is rather straightforward and based on different unambiguous and independent experimental results due to the polarization dependence of the SEXAFS technique and the possibility of probing independently the environment of different atom types. From the S K-edge data we know that the S atom of SO is located in fourfold hollow sites with an S–Cu bond length of 2.36 ± 0.05 Å. The rather large error bar here results from the poor statistics of the S K-edge data. Both the S and O K-edge analysis show (independently) that the SO species lie flat on the surface with an accuracy of about 10°. In order to find the O locations (O in SO and atomic O) we have to simulate the O K-edge data. Ahead of any simulation we can, in principle, determine the intramolecular bond length by just analysing the O–S Fourier peak. From the amplitude ratio $A(90°)/A(20°)$ of the nn O–Cu peak, on the other hand, we learn that the average oxygen location must be close to a bridge site and from XPS we know the approximate relative amounts of atomic O and O in SO. A least-squares fitting of the SEXAFS $\chi(k)$ functions assuming atomic oxygen in a high-symmetry site then yields the correct O location (see figure 17) with the corresponding bond

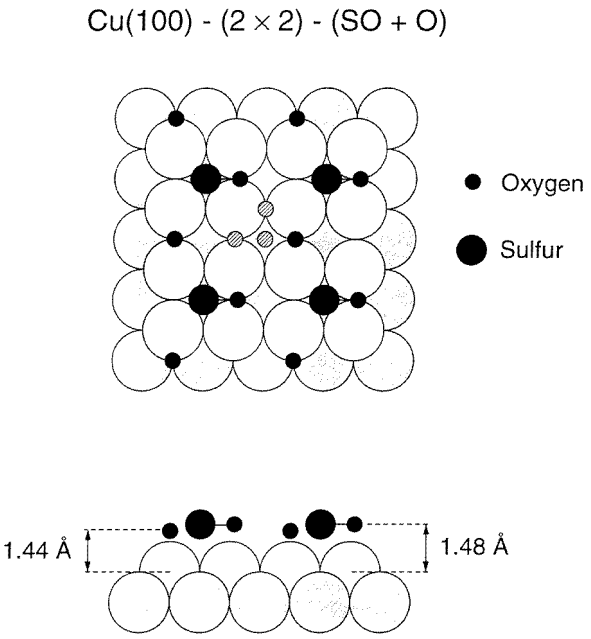

Figure 17. A model of a Cu(100)–(2 × 2)–(SO + O) structure with the local geometry of the oxygen and SO species deduced from SEXAFS [12]. Excluded atomic O positions (see text) are marked as shaded small circles. The real surface with the (SO–2O+S) phase must contain more atomic oxygen and less SO that shown here and in addition some atomic sulphur (see text).

lengths and experimental errors noted above. We should mention, however, that we can safely exclude atomic oxygen locations in hollow sites marked with shaded small circles in figure 17. The only other Fourier peak (except the O–S and the nn O–Cu peak) sticking out of the noise level in figure 16, peak B, cannot be reproduced by atomic oxygen in hollow sites in which O atoms on the clean Cu(100) are adsorbed [28] and cannot be explained by a multiple-scattering path. Co-adsorbed atomic O in bridge sites (shaded small circles) different from those depicted in figure 17 as full circles can also be excluded. They worsen the fit of the SEXAFS $\chi(k)$ functions in figure 16 and result in unphysically (according to experience) low O–O(SO) distances ($\leqslant 2.49$ Å). The repulsion between the oxygen atoms might also be the reason for the experimental result that hollow-site adsorption does not occur (O–O(SO) $= 2.78$ Å for atomic O in hollow sites).

A final question which needs to be addressed concerns the intromolecular bond length of SO. The measured value of 1.41 ± 0.03 Å is different from that of neutral SO (1.48 Å) but close to that of SO^+ (1.42 Å) [14]. This raises the general question of the charge state of the adsorbed sulphur oxides which has not yet been thoroughly discussed in the literature. As far as surface SO_3 and SO_4 species on Ag(110) are concerned, it is assumed that they are in the dianion form [22].

10. Conclusions

The main part of this review was devoted to the geometry of SO_2 surface complexes. The few structural studies performed to date on SO_2 adsorption on metal surfaces already display part of the diversity of bonding modes known from transition-metal complexes.

Quantitative structural analyses, however, turn out to be rather demanding, partly due to the fact that co-adsorbed atomic oxygen and sulphur as well as other SO_x ($x \neq 2$) species have to be taken into account. The determined parallel orientations of SO_2 molecules adsorbed on Ni(110), Ni(100) and Ni(111) with S atoms in bridge sites are surprising at first sight, but for all the systems discussed here there seems to be a qualitative understanding of the SO_2–metal bond by just looking at the energy, symmetry and spatial extension of substrate orbitals which can interact with the HOMO and LUMO of SO_2. To completely understand the bonding of SO_2 to metal surfaces, however, calculations are very necessary for SO_2 in all its possible configurations and adsorption sites.

Acknowledgments

The author would like to acknowledge the contributions of B Brena, D Cocco, G Comelli, J Feldhaus, B Itchkawitz, G Jäkisch, H M Koppe, N Pangher, G Paolucci, M Polcik and L Wilde to the own work reviewed here. It is a pleasure to thank T Ohta for permission to reproduce figures from publications of his group. The work was supported by the German Federal Ministry of Education, Science, Research and Technology (BMBF) under contract No 05 625EBB 9.

References

[1] Homer 1925 *Odyssey* (London: Chiswick) p 348
[2] Oudar J 1980 *Catal. Rev. Sci. Eng.* **22** 171
[3] Ryan B R, Kubas G J, Moody D C and Eller P G 1981 *Struct. Bonding* **46** 47
[4] Zebisch P, Weinelt M and Steinrück H-P 1993 *Surf. Sci.* **295** 295
[5] Bradshaw A M 1995 *Surf. Sci.* **331–333** 978
[6] Burke M L and Madix R J 1988 *Surf. Sci.* **194** 223
[7] Solomon J L, Madix R J, Wurth W and Stöhr J 1991 *J. Phys. Chem.* **95** 3687
[8] Outka D A, Madix R J, Fisher G B and DiMaggio C 1986 *Langmuir* **2** 406
[9] Sun Y-M, Sloan D, Alberas D J, Kovar M, Sun Z-J and White J M 1994 *Surf. Sci.* **319** 34
[10] Yokoyama T, Terada S, Yagi S, Imanishi A, Takenaka S, Kitajima Y and Ohta T 1995 *Surf. Sci.* **324** 25
[11] Terada S, Imanishi A, Yokoyama T, Takenaka S, Kitajima Y and Ohta T 1995 *Surf. Sci.* **336** 55
[12] Pangher N, Wilde L, Polcik M and Haase J 1997 *Surf. Sci.* **372** 211
[13] Clark A H and Beagley B 1971 *Trans. Faraday Soc.* **67** 2216
[14] Zitterer H *et al* (eds) 1980 *Gmelin Handbuch der anorganischen Chemie, S, Erg.* vol 3 (Berlin: Springer) p 1
[15] Roos B and Siegbahn P 1971 *Theor. Chim. Acta* **21** 368
[16] Sze K-H, Brion C E, Tong X-M and Li J-M 1987 *Chem. Phys.* **115** 433
[17] Rodriguez J A 1990 *Surf. Sci.* **226** 101
[18] Blyholder G 1974 *Surf. Sci.* **42** 249
[19] Tronc M, Azria R and LeCoat Y 1980 *J. Phys. B: At. Mol. Phys.* **13** 2327
[20] Sakaki S, Sato H, Imai Y, Morokuma K and Ohbuko K 1985 *Inorg. Chem.* **24** 4538
[21] Haase J 1996 *J. Chem. Soc. Faraday Trans.* **92** 1653
[22] Outka D A and Madix R A 1984 *Surf. Sci.* **137** 242
[23] Ahner J, Effendy A, Vajen K and Wassmuth H-W 1990 *Vacuum* **41** 98
[24] Höfer M, Stolz H and Wassmuth H-W 1992 *Surf. Sci.* **272** 342
[25] Köhler U and Wassmuth H-W 1983 *Surf. Sci.* **126** 448
[26] Polcik M, Wilde L, Haase J, Brena B, Cocco D, Comelli G and Paolucci G 1996 *Phys. Rev.* B **53** 13 720
[27] Leung K T, Zhang X S and Shirley D A 1989 *J. Phys. Chem.* **93** 6164
[28] Lederer T, Arvanitis D, Comelli G, Tröger L and Baberschke K 1993 *Phys. Rev.* B **48** 15 390
[29] Horsley J A 1988 *Chemistry and Physics of Solid Surfaces (Springer Series in Surface Science 10)* ed V R Vanselow and R Howe (Berlin: Springer)
[30] Gutiérrez-Sosa A, Walsh J F, Muryun C A, Finetti P, Thornton G, Robinson A W, D'Addato S and Frigo S P 1996 *Surf. Sci.* **364** L519
[31] 1994 *Landolt–Börnstein New Series* Group III, vol 24b ed G Chiarotti (Berlin: Springer)

[32] Burke M L and Madix R J 1988 *J. Vac. Sci. Technol.* A **6** 789
[33] Astegger S and Bechtold E 1982 *Surf. Sci.* **122** 491
[34] Höfer M, Hillig S and Wassmuth H-W 1990 *Vacuum* **41** 102
[35] Köhler U and Wassmuth H-W 1982 *Surf. Sci.* **117** 668
[36] Lee P A, Citrin P H, Eisenberger P and Kincaid B M 1981 *Rev. Mod. Phys.* **53** 769
[37] Citrin P H, Eisenberger P and Kincaid B M 1976 *Phys. Rev. Lett.* **36** 1346
[38] Somers J S, Lindner T, Surman M, Bradshaw A M, Williams G P, McConville C F and Woodruff D P 1987 *Surf. Sci.* **183** 576
[39] Stöhr J 1992 *NEXAFS Spectroscopy* ed G Ertl, R Gomer, D L Mills and H K V Lotsch (Berlin: Springer)
[40] Feldhaus J, Schaefers F and Peatman W 1987 *SPIE Proc.* **733** 242
[41] Bodeur S and Esteva J M 1985 *Chem. Phys.* **100** 415
[42] Pangher N, Itchkawitz B, Köppe H M, Feldhaus J and Haase J 1993 *Phys. Rev. Lett.* **71** 4365
[43] Wilde L, Polcik M and Haase J 1997 *Surf. Sci.* at press
[44] Warburton D R, Thornton G, Norman D, Richardson C H, McGrath R and Sette F 1987 *Surf. Sci.* **189/190** 495
[45] McGrath R, MacDowell A A, Hashizume T, Sette F and Citrin P H 1990 *Phys. Rev. Lett.* **64** 575
[46] The inclination angles of about 20° (⟨110⟩) and 28° (⟨100⟩) quoted in [11] for the π^* resonance analyses must be wrong. The vanishing π^* resonance intensity at $\theta = 90^\circ$ immediately suggests flat-lying molecules (the π^* orbitals are polarized perpendicular to the molecular planes), i.e., an inclination angle of 90°. The same holds for the inclination angles on Ni(111) and Ni(100) [10].